EFFECT OF THE PROCESSING AND TRANSPORT PARAMETERS ON MOLD FILLING IN ROLL-TO-ROLL NANOIMPRINT LITHOGRAPHY

J. P. Gomez-Constante, P. R. Pagilla[1], and K. R. Rajagopal

Department of Mechanical Engineering
Texas A&M University, College Station, TX
USA

ABSTRACT

Based on a model developed for the roll-to-roll imprinting process, this paper describes the relative importance of the processing, material properties, and transport parameters in Roll-to-Roll Nanoimprint Lithography (R2RNIL). In particular, the model is utilized to investigate the effect of web speed, fluid film thickness, viscosity, stress relaxation time, mold pattern geometry and size on mold filling. Based on a typical imprint roller configuration, kinematic analysis, and the conservation laws from classical mechanics, the behavior of the squeezing of a viscoelastic fluid film into a rigid mold cavity is described. Further, the effect of web speed, fluid film thickness and key rheological parameters, namely the Weissenberg and Deborah numbers, are discussed. These dimensionless numbers are typically employed to quantify viscoelastic effects in fluid flow problems. The effect of other scale-sensitive and geometric parameters, such as the capillary number and pattern width-to-height ratio, on the imprint process is also discussed. Numerical simulations are provided to corroborate the discussions and to quantify the relative importance of the parameters.

1 INTRODUCTION

Roll-to-Roll Nanoimprinting Lithography (R2RNIL) is a process of imprinting nanoscale patterns continuously on a moving surface. Since the patterns are continuously produced on the surface, R2RNIL has many potential advantages over batch imprinting, including efficient and cost-effective mass production of large-area imprinted surfaces. In a typical R2RNIL process, a coated web is passed through the nip of two rollers with one roller surface containing the mold of the imprint pattern that needs to be transferred to the coated side of the web. In one form of R2RNIL, the substrate is coated with a viscoelastic fluid and transported into the imprinting process. There are two phases of operation in the imprinting process: (1) the mold filling phase where the coated fluid is squeezed

[1]Corresponding author email: ppagilla@tamu.edu.

into the mold pattern at the entry of the nip of the two rollers and (2) the curing phase where the filled fluid in the mold is cured or solidified using a heating source. Although there have been empirical observations and developments related to explaining the mold filling operation, the factors affecting mold filling from the mechanics viewpoint have not been systematically investigated. The focus of this work is on advancing such an understanding by providing insights into how key process and transport parameters affect mold filling based on a model developed by the authors.

With the ever increasing need for better manufacturing processes while improving productivity and lowering costs, R2RNIL is one suitable manufacturing process for surface patterning due to its high throughput and mass production capabilities. Even though similar processes such as embossing and macroscale patterning have been employed for quite some time in the industry, there are still many open problems, especially for imprinting patterns at the nanoscale. One aspect that is key to large area patterning is to improve the quality of the imprinted features at reasonable web speeds (≥ 5 m/min). To address this aspect of the R2RNIL process, this paper focuses on the effects of web speed, fluid film thickness, geometry of the mold, and other material and physical parameters that are critical to mold filling, and aims to determine the connections between these parameters.

In an attempt to develop a R2R configuration that is capable of producing quality imprinting patterns, several different configurations of R2RNIL have been proposed in the literature. From the geometric disposition of the rollers, mold and the coated substrate, one can identify the following four main configurations as illustrated in Fig. 1[1]: (i) Basic R2RNIL: a roller containing the mold pattern is just pressed against the coated substrate without any wrap. (ii) Wrapped R2RNIL: a roller indented with the mold pattern is pressed against a flexible substrate and partially wrapped around the mold roller, increasing the contact area in between the mold and the substrate. (iii) Belt R2RNIL: a flexible mold is wrapped around two rollers effectively increasing the contact area between the mold and the coated substrate. (iv) Step R2RNIL: a mold carved on a flat plate is pressed against the coated substrate to obtain a batch of imprinted features at a time.

In any configuration, the aim is to ensure that the geometry of the mold feature is properly transferred to the coated substrate; this involves filling the mold with the fluid film on the substrate, phase change from liquid to solid, and then debonding of the patterned substrate from the mold roller. From the phase-change viewpoint, R2RNIL can be divided into two main categories: Thermal NIL and UV NIL. In thermal NIL, a polymer substrate is heated until its surface reaches glass transition temperature (350-400 F) in order to decrease the mechanical properties so that the mold can be appropriately filled; the phase change occurs when the polymer is cooled down back to room temperature. On the other hand, UV NIL consists of a low viscosity photo-sensitive fluid film at room temperature or slightly elevated than the room temperature that is pushed inside the cavity of the mold. The phase-change process is a photo-chemical phenomenon that is triggered by irradiation of the surface by a UV light source.

[1] classification and figure reproduced from [7]

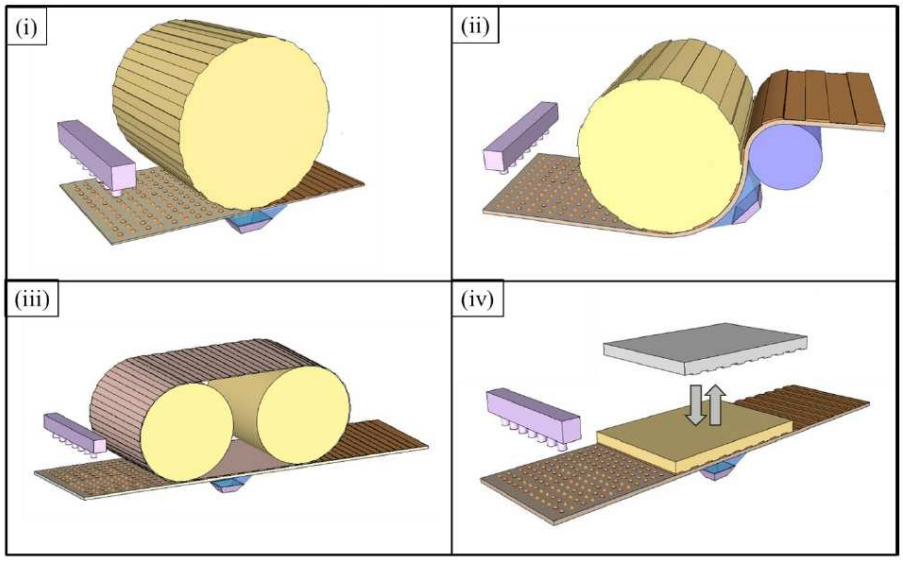

Figure 1 – Typical configurations of R2RNIL: (i) Basic, (ii) Wrapped, (iii) Belt, and (iv) Step.

The UV NIL process is known to have several advantages over thermal NIL including smaller nip forces, does not require elevated temperatures and pressures, and does not involve the complex heat transfer process during phase change. We will consider UV NIL with wrapped configuration as shown in Fig. 1(ii).

Attempts to model the mold filling process can be traced back to the problem of squeezing flow between two solid parallel plates [1]; the early ideas have led to many perturbation methods that were useful for understanding the basic problems of the process. Schift and Heyderman [2] employed the squeezing flow model with some correction factors which accounted for the geometry of the mold cavity and the viscous nature of the fluid to derive a governing equation for the evolution of the height of the fluid film; from this equation, a quantity called the filling time t_{fill} was obtained which the authors claim represents the time it takes the fluid film to fill the cavity of the mold. Using the same basic ideas, some recent models account for slip on the solid boundaries of the mold surface (Kim et al. [3] and Young [4]), but with an oversimplification of the physics that underlies the process, for instance not taking into account any viscoelastic behavior.

Recently, more sophisticated models based on conservation laws have been developed, where the viscoelastic nature of the fluid film has been taken into account. Ahn and Guo [5] derived a model for predicting the Residual Layer Thickness (RLT) of a batch imprinting process with a Newtonian fluid with high viscosity to compensate for the viscoelastic behavior. Jain and Bonnecaze [6] employ a viscoelastic model, namely the Upper Convected Maxwell, along with a perturbation of the velocity and pressure fields in terms of the Deborah Number to account for the viscoelastic behavior.

The existing models for the R2R process have similar deficiencies as the batch

imprinting process – lack of physical compliance with conservation laws and material properties, consideration of the free surface that is being formed inside the mold, and the evolutionary nature of the problem. We aim to address some of these gaps through the development of a model and its subsequent analysis via representative numerical simulations. Another aspect that is missing in the previous approaches is the clear distinction between mold filling and phase change, which occur sequentially in most configurations and must be treated as such in model development. The modeling approach followed in this paper allows for such a distinction, although the focus in this paper is on mold filling.

Experimental evidence also suggests that at high web speeds the geometry of the imprinted features is not satisfactory, and the problem gets even worse at higher speeds. For instance, the most relevant and recent achievements in R2RNIL are summarized in Table 1[2].

Table 1 – Recent achievements in UV and Thermal R2RNIL

Citation	**System Type**	**Critical dimension**	**RLT**	**Web width**	**Web speed**	**Pattern accuracy**
Thesen *et al.* [8], [9]	UV R2RNIL	500 nm width /200 nm height	N.R.	300 mm	30 m/min	94%
Wu [10]	UV R2RNIL	50 nm width /180 nm height	66 nm	50 mm	1 m/min	95%
Inanami *et al.* [11]	UV R2RNIL	24 nm width /58 nm height	13 μm	70 mm	1 m/min	N.R.
Ahn *et al.* [12]	UV R2RNIL	50 nm width	N.R.	300 mm	>1 m/min	N.R.
Ahn *et al.* [13]	UV R2RNIL	50 nm width	12 nm	80 mm	N.R.	N.R.
Mäkelä *et al.* [14]	Thermal R2RNIL	400 nm width /230 nm height	N.R.	50 mm	20 m/min	50%
Sohn *et al.* [15]	Thermal R2RNIL	5 μm width	N.R.	150 mm	1.8 m/min	N.R.

The rest of the paper is organized as follows. In Section 2, we describe the kinematic relations along with the Conservation Laws to determine a system of governing equations for mold filling. We also discuss the relative importance of the various dimensionless numbers (Reynolds, Weissenberg, Deborah and Capillary numbers) which are affected by the fluid film properties and web speed. In Section 3, we discuss the numerical simulations of the integro-differential governing equations where the solution is obtained by employing the classical Marker and Cell (MAC) scheme. The conclusions of this work and directions for future work are provided in Section 4.

[2]Table information partially reproduced from the one shown in [7].

2 MODEL DESCRIPTION

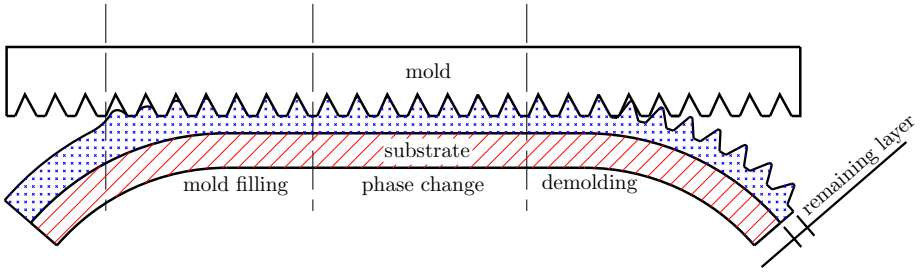

Figure 2 – Illustration of the R2RNIL sub-processes

The nanoimprinting process can be divided into three sub-processes as illustrated in Fig. 2. (1) Mold filling process: the fluid film is pushed into the mold cavity to obtain the desired geometry. (2) Phase change process: change of phase of the fluid film, including the filled mold, from liquid to solid state. (3) Demolding process: the web with patterned surface is demolded from the mold. Note that the various configurations illustrated in Fig. 1 contain these sub-processes with some variations in terms of the duration and/or superposition between sub-processes. Thus, the developments in this paper are applicable to all these configurations.

2.1 Kinematics

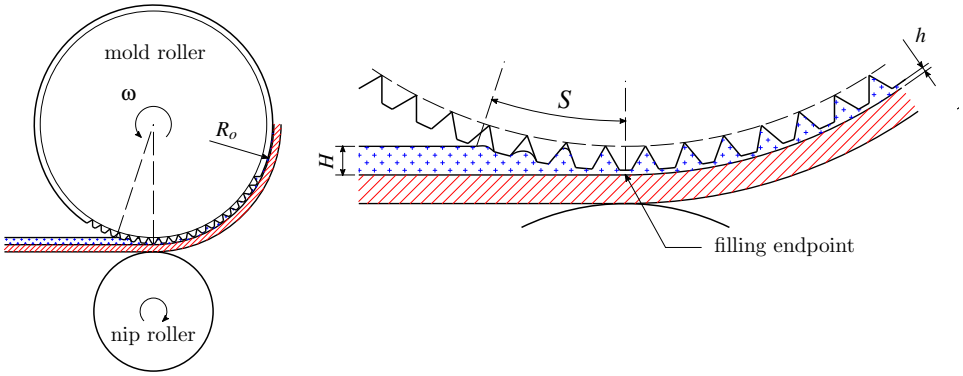

Figure 3 – Kinematics of continuous imprinting

Figure 3 illustrates the geometry of the coated web entering the imprint rollers with the following definitions of the key elements and parameters: a mold roller containing the pattern on its surface with outer radius R_o and rotating at a constant angular speed ω; a nip roller rotating at the same angular speed but in the opposite direction; H denotes the coating fluid thickness on the substrate prior to the fluid making contact with the mold roller; and h denotes the remaining layer film thickness. A submerged arc of length S is generated in between the point where the outer radius of the mold roller touches the surface of the fluid film and the endpoint of filling in between the roller and substrate; this arc S is the

only portion of the contact length in which the fluid can fill the mold pattern due to the relative motion between the rollers that is perpendicular to the plane of the substrate.

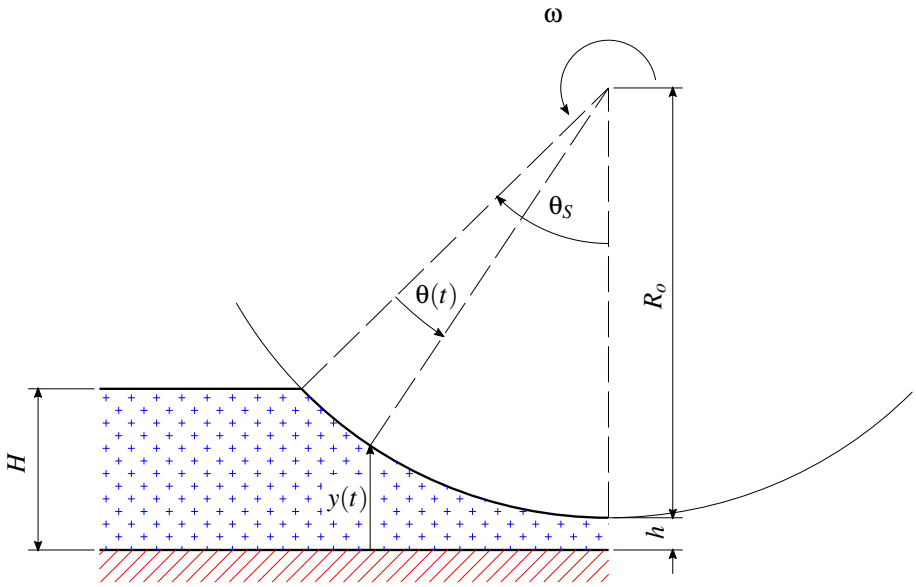

Figure 4 – Vertical position of the pattern $y(t)$ in arc S

Considering the endpoint of mold filling as the zero vertical reference (see Fig. 4) and assuming that there is no slip between the nip roller and the substrate, the vertical distance between a material point on the external circumference of the mold roller (within the arc S) and the coated substrate is given by

$$\begin{aligned} y(t) &= h + R_o - R_o \cos\left(\theta_S - \theta(t)\right) \\ &= h + R_o - R_o \cos\left(\frac{S}{R_o} - \omega t\right) \end{aligned} \quad \{1\}$$

where θ_S is the angle subtended by the arc S, $\theta(t)$ is angle of a material point under consideration on the mold roller at the vertical distance $y(t)$, and ω is the angular speed of the mold roller. Note that at $t = 0$ we have

$$H = h + R_o - R_o \cos\left(\frac{S}{R_o}\right). \quad \{2\}$$

Substituting S from Eq. 2 into Eq. 1 yields:

$$\begin{aligned} y(t) &= h + R_o \left[1 - \cos\left(\arccos(1 - \frac{H-h}{R_o}) - \omega t\right)\right] \\ &= h + R_o \left[1 - \left(1 - \frac{H-h}{R_o}\right)\cos(\omega t) - \sqrt{1 - \left(1 - \frac{H-h}{R_o}\right)^2}\sin(\omega t).\right] \end{aligned} \quad \{3\}$$

The available time for filling, denoted by T_1, is the time it takes for a material point on the free surface of the fluid to travel across the arc S; this is obtained by setting the time derivative of $y(t)$ to zero:

$$T_1 = \frac{1}{\omega} \arctan \left[\frac{\sqrt{1 - \left(1 - \frac{H-h}{R_o}\right)^2}}{1 - \frac{H-h}{R_o}} \right]. \qquad \{4\}$$

From the viewpoint of the vertical motion, the pattern on the mold roller approaches the fluid on the substrate; the vertical displacement of the material point on the mold roller after making contact with the fluid film, denoted by $u_s(t)$, is related to $y(t)$ as $u_s(t) = H - y(t)$. Thus, we obtain

$$u_s(t) = R_o \left[\left(1 - \frac{H-h}{R_o}\right) \cos(\omega t) + \sqrt{1 - \left(1 - \frac{H-h}{R_o}\right)^2} \sin(\omega t) - 1 \right] + H - h. \qquad \{5\}$$

This formulation allows us to mimic the roll-to-roll imprinting process of two parallel plates with the plate containing the fluid film approaching the plate containing the mold pattern; this formulation is primarily employed for numerical simulations of mold filling. Note that for any time past the available time for filling T_1, the relative displacement between the mold roller and the nip roller is given by the thickness of the residual layer of the film and the base substrate; this is illustrated in Fig. 5.

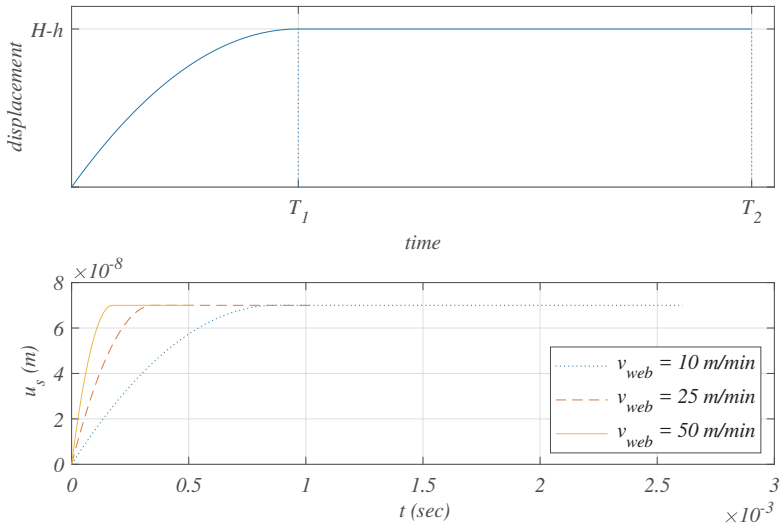

Figure 5 – Evolution of the displacement function $u_s(t)$ (top); $u_s(t)$ for different web speeds (bottom)

Let us now focus on one pattern of the roller; we will assume that mold filling in any pattern is not significantly affected by mold filling in adjacent patterns.

Because nanoscale patterns are considered, it is reasonable to assume that the radius of the mold roller is much larger than the thickness of the fluid film, that is, $0 < H << R_o$. Let L be the arc subtended by one pattern. The domain for the mold filling process for each pattern has width L and height H as illustrated in Fig. 6 at the beginning of the arc of contact S. This domain evolves as the fluid is filled into the mold pattern caused by the relative motion given by $u_s(t)$.

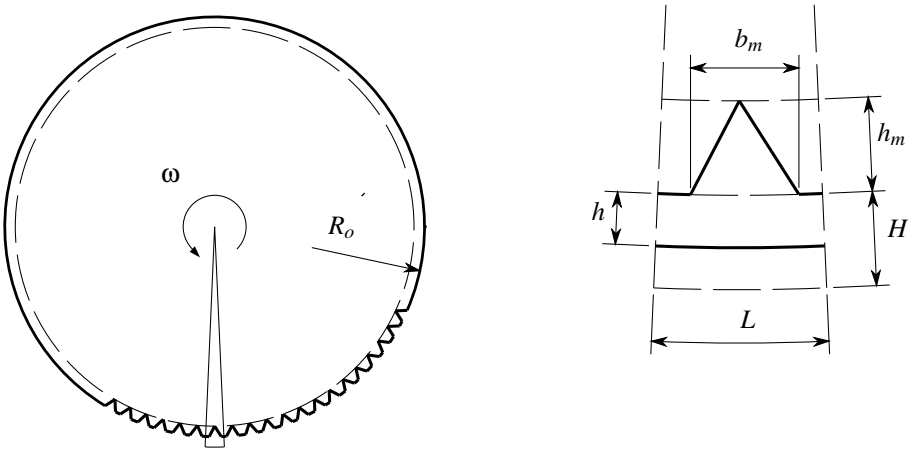

Figure 6 – Problem domain for one pattern

The bidimensional nature of the problem (with the assumption that the filling is similar on any parallel cross-section along the web width) and the imcompressibility assumption imply that the area filled in the mold cavity should be approximately equal to the total area displaced by the substrate. That is, with regard to the pattern width (b_m) and height (h_m), one can make the following approximation:

$$\frac{1}{2} b_m h_m \approx L(H-h). \qquad \{6\}$$

We can also note that the width of the domain L is much smaller than the mold roller radius and the length of the arc S. Thus, the domain under consideration for each pattern resembles that of a rectangle of width L and height H. Moreover, since the web width is very large compared to the size of the features, the relative motion of the mold roller and substrate with fluid film can be approximated by the two infinite parallel plates in the batch imprinting process (Fig. 7). Note that, at this scale, we are assuming that the interaction of the fluid from one pattern domain to the other can be ignored during filling; study of this interaction may be relevant and will be considered in future developments.

2.2 Application of Conservation Laws to R2RNIL Process

In this study, we will assume the fluid behavior to follow a linearized version of the Upper Convected Maxwell fluid (see for instance [16] or [17]) which we plan to use in a more detailed future study that allows for large strains. To start, recall

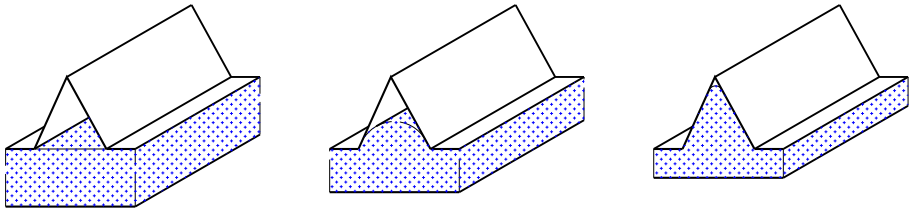

Figure 7 – Evolution of the fluid filling in the mold pattern

the conservation of linear momemtum, angular momentum and mass given by:

$$\rho \frac{d\vec{v}}{dt} = \text{div } \mathbb{T}^T + \rho \vec{b} \qquad \{7\}$$

$$\mathbb{T} = \mathbb{T}^T \qquad \{8\}$$

$$\frac{\partial \rho}{\partial t} + \text{div } (\rho \vec{v}) = 0 \qquad \{9\}$$

along with the (Upper Convected Maxwell) constitutive equation given by

$$\lambda \overset{\triangledown}{\mathbb{T}}_d + \mathbb{T}_d = 2\mu \mathbb{D} \qquad \{10\}$$

where ρ is the density of the fluid, $\vec{b}$ is the body force field, λ is the stress-relaxation time, $\mathbb{T}$ is the Cauchy stress, and $\mathbb{T}_d$ is the deviatoric part of the Cauchy stress. Next, let us define the displacement vector field $\vec{u}$ which is related to the velocity field $\vec{v}$ by

$$\frac{d\vec{u}}{dt} = \vec{v}. \qquad \{11\}$$

Substituting Eq. {11} into the conservation laws, neglecting the body forces $\vec{b}$, and assuming that the fluid is imcompressible, we obtain

$$\rho \frac{d^2\vec{u}}{dt^2} = \text{div } \mathbb{T}, \qquad \{12\}$$

$$\text{div } \vec{v} = 0. \qquad \{13\}$$

Now, assuming that the Frobenius norm of the displacement gradient is small (i.e. $\|\nabla \vec{u}\| << 1$), we can linearize the conservation laws and the constitutive equation resulting in the following equations:

$$\rho \frac{\partial^2 \vec{u}}{\partial t^2} = -\text{grad } p + \text{div } \mathbb{T}_d \qquad \{14\}$$

$$\text{div } \vec{u} = 0, \qquad \{15\}$$

$$\lambda \frac{\partial \mathbb{T}_d}{\partial t} + \mathbb{T}_d = 2\mu \frac{\partial}{\partial t}(\text{grad } \vec{u} + \text{grad } \vec{u}^T). \qquad \{16\}$$

Let the Cartesian components of the displacement vector be denoted by $\vec{u} = (u_x, u_y)$. Using the Cartesian coordinate system and replacing the deviatoric

part of the Cauchy stress (from the linearized constitutive relation) into the linearized conservation of linear momentum we obtain

$$\rho \frac{\partial^2 u_x}{\partial t^2} = -\frac{\partial p}{\partial x} + \frac{\mu}{\lambda} e^{t/\lambda} * d(\Delta u_x) \quad \{17\}$$

$$\rho \frac{\partial^2 u_y}{\partial t^2} = -\frac{\partial p}{\partial y} + \frac{\mu}{\lambda} e^{t/\lambda} * d(\Delta u_y) \quad \{18\}$$

$$\frac{\partial u_x}{\partial x} + \frac{\partial u_y}{\partial y} = 0 \quad \{19\}$$

where the '$*$' denotes the convolution operator defined by

$$e^{t/\lambda} * d(\Delta \vec{\mathbf{u}}) = \int_0^t e^{-\frac{t-s}{\lambda}} \frac{\partial}{\partial s} (\Delta \vec{\mathbf{u}}(s))\, ds.$$

To write the governing equations in terms of dimensionless variables, we define the following non-dimensional variables:

$$\bar{x} = \frac{x}{L}, \qquad \bar{y} = \frac{y}{H}, \qquad \bar{t} = \frac{t}{T_1},$$
$$\bar{u}_x = \frac{u_x}{L}, \qquad \bar{u}_y = \frac{u_y}{H}, \qquad \bar{p} = \frac{\lambda}{\mu} p,$$
$$Wi = \frac{\lambda v_s(0)}{H}, \qquad De = \frac{\lambda}{T_1}, \qquad Re = \frac{\rho v_s(0) H}{\mu}$$

where $v_s(0)$ is given by

$$v_s(0) = \frac{d}{dt} (u_s(t)) \bigg|_{t=0}.$$

The Weissenberg number Wi is the ratio of the viscous forces to the elastic forces, the Deborah number De is the ratio of the stress-relaxation time to the time scale of the process [18], and Re is the usual Reynolds number. In non-dimensional variables, the governing equations may be written as

$$\frac{ReDe^2}{Wi} \frac{\partial^2 \bar{u}_x}{\partial \bar{t}^2} = e^{-\frac{\bar{t}}{De}} * d \left[\left(\frac{H}{L} \right)^2 \frac{\partial^2 \bar{u}_x}{\partial \bar{x}^2} + \frac{\partial^2 \bar{u}_x}{\partial \bar{y}^2} \right] - \left(\frac{H}{L} \right)^2 \frac{\partial \bar{p}}{\partial \bar{x}} \quad \{20\}$$

$$\frac{ReDe^2}{Wi} \frac{\partial^2 \bar{u}_y}{\partial \bar{t}^2} = e^{-\frac{\bar{t}}{De}} * d \left[\left(\frac{H}{L} \right)^2 \frac{\partial^2 \bar{u}_y}{\partial \bar{x}^2} + \frac{\partial^2 \bar{u}_y}{\partial \bar{y}^2} \right] - \frac{\partial \bar{p}}{\partial \bar{y}} \quad \{21\}$$

$$\frac{\partial \bar{u}_x}{\partial \bar{x}} + \frac{\partial \bar{u}_y}{\partial \bar{y}} = 0. \quad \{22\}$$

Because of the scale of the fluid within the mold pattern, we have to consider the effect of the surface forces and their influence on the evolution of the fluid film surface within the mold pattern. Taking this into account, the conservation of linear momentum for the free surface of the fluid film is given by

$$\rho (\vec{v} \cdot \hat{n}) \vec{v} = (\mathbb{T}_{\text{air}} - \mathbb{T}) \hat{n} + \gamma (\text{div}_t\ \hat{n}) \hat{n} \quad \{23\}$$

where γ is the surface energy, the operator div_t is the divergence operator defined on the free surface, and $\hat{n}$ is the normal unit vector in the free surface. By a very

similar process of linearization and non-dimensionalization to what was done previously, and by neglecting the effect of the air, we can obtain the following governing equations that include the effect of surface forces:

$$\frac{ReDe^2}{Wi}\frac{\partial \bar{u}_x}{\partial \bar{t}}\left(\frac{\partial \bar{u}_y}{\partial \bar{t}}\right) = -e^{-\frac{\bar{t}}{De}} * d\left[\frac{\partial \bar{u}_x}{\partial \bar{y}} + \left(\frac{H}{L}\right)^2 \frac{\partial \bar{u}_y}{\partial \bar{x}}\right] \quad \{24\}$$

$$\frac{ReDe^2}{Wi}\left(\frac{\partial \bar{u}_y}{\partial \bar{t}}\right)^2 = \bar{p} - 2e^{-\frac{\bar{t}}{De}} * d\left[\frac{\partial \bar{u}_y}{\partial \bar{y}}\right] + \frac{Wi}{Ca}\left(\frac{H}{L}\right)^2 \frac{\partial^2 \bar{u}_y}{\partial \bar{y}^2} \quad \{25\}$$

where the capillary number Ca, which is the ratio of the surface force to the viscous force, is given by

$$Ca = \frac{v_s(0)\mu}{\gamma}.$$

3 NUMERICAL SIMULATION RESULTS

Let $\Omega = (-\frac{1}{2}, \frac{1}{2}) \times (-1, 0) \subset \mathbb{R}^2$ be the spatial domain, and $I_t = (0,1) \subset \mathbb{R}$ the time interval in which the available time for filling takes place. Set $\Omega_t = \Omega \times I_t$ as the evolution of the domain in time. The imprinting process is then given by the linear system of partial differential equations

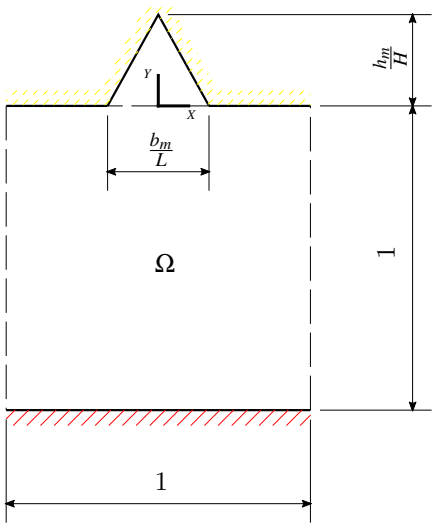

Figure 8 – Spatial domain for numerical computations

$$\frac{ReDe^2}{Wi}\frac{\partial^2 \bar{u}_x}{\partial \bar{t}^2} - e^{-\frac{\bar{t}}{De}} * d\left[\left(\frac{H}{L}\right)^2 \frac{\partial^2 \bar{u}_x}{\partial \bar{x}^2} + \frac{\partial^2 \bar{u}_x}{\partial \bar{y}^2}\right] + \left(\frac{H}{L}\right)^2 \frac{\partial p}{\partial \bar{x}} = 0 \qquad \text{in } \Omega_t \quad \{26\}$$

$$\frac{ReDe^2}{Wi}\frac{\partial^2 \bar{u}_y}{\partial \bar{t}^2} - e^{-\frac{\bar{t}}{De}} * d\left[\left(\frac{H}{L}\right)^2 \frac{\partial^2 \bar{u}_y}{\partial \bar{x}^2} + \frac{\partial^2 \bar{u}_y}{\partial \bar{y}^2}\right] + \frac{\partial \bar{p}}{\partial y} = 0 \qquad \text{in } \Omega_t \quad \{27\}$$

$$\frac{\partial \bar{u}_x}{\partial \bar{x}} + \frac{\partial \bar{u}_y}{\partial \bar{y}} = 0 \qquad \text{in } \Omega_t \quad \{28\}$$

$$\bar{u}_x = \bar{u}_y = \bar{p} = 0 \quad \text{in } \Omega \times \{0\} \quad \{29\}$$

$$\frac{\partial \bar{u}_x}{\partial \bar{t}} = \frac{\partial \bar{u}_y}{\partial \bar{t}} = 0 \quad \text{in } \Omega \times \{0\} \quad \{30\}$$

with periodic boundary conditions on the sides of the spatial domain, upper and lower dynamic boundary conditions, which are given by

$$\frac{ReDe^2}{Wi}\frac{\partial \bar{u}_x}{\partial \bar{t}}\left(\frac{\partial \bar{u}_y}{\partial \bar{t}}\right) + e^{-\frac{\bar{t}}{De}} * d\left[\frac{\partial \bar{u}_x}{\partial \bar{y}} + \left(\frac{H}{L}\right)^2 \frac{\partial \bar{u}_y}{\partial \bar{x}}\right] = 0 \qquad \text{on } \left(-\frac{b_m}{2L}, \frac{b_m}{2L}\right) \times \{0\} \times I_t \quad \{31\}$$

$$\frac{ReDe^2}{Wi}\left(\frac{\partial \bar{u}_y}{\partial \bar{t}}\right)^2 + 2e^{-\frac{\bar{t}}{De}} * d\left[\frac{\partial \bar{u}_y}{\partial \bar{y}}\right] + \frac{Wi}{Ca}\left(\frac{H}{L}\right)^2 \frac{\partial^2 \bar{u}_y}{\partial \bar{y}^2} - \bar{p} = 0 \qquad \text{on } \left(-\frac{b_m}{2L}, \frac{b_m}{2L}\right) \times \{0\} \times I_t \quad \{32\}$$

$$\bar{u}_x = 0 \qquad \text{on } \left(-\frac{1}{2}, \frac{1}{2}\right) \times \{-1\} \times I_t \quad \{33\}$$

$$\bar{u}_y = \bar{u}_s(t) \quad \text{on } \left(-\frac{1}{2}, \frac{1}{2}\right) \times \{-1\} \times I_t \quad \{34\}$$

The restriction in the displacement of the free surface of the mold is defined by

$$\bar{y} = \left[\frac{h_m}{H} - \frac{2h_m L}{bmH}\,|\bar{x}|\right] \mathcal{H}\left(\frac{h_m}{H} - \frac{2h_m L}{b_m H}\,|\bar{x}|\right). \quad \{35\}$$

where $\mathcal{H}$ is the Heaviside step function. Notice that the boundary conditions are only given in terms of the components of the displacement, which means that the pressure field is completely determined by the application of the conservation laws only.

The resulting governing equations are then numerically solved using an algorithm which was implemented in MATLAB®. The simplicity of the domain allows us to use finite differences instead of finite elements. Moreover, the finite difference method is more robust for solving the class of problems under consideration in rectangular domains since we can take the advantage of the Marker and Cell (MAC) scheme [19] that automatically satisfies the finite-dimensional $inf - sup$ condition and guarantees not only the existence and uniqueness of solutions of the numerical approximation but also ensures that the approximation converges (as the mesh size becomes smaller) to the actual solution. Nevertheless, some complications were found with regard to the

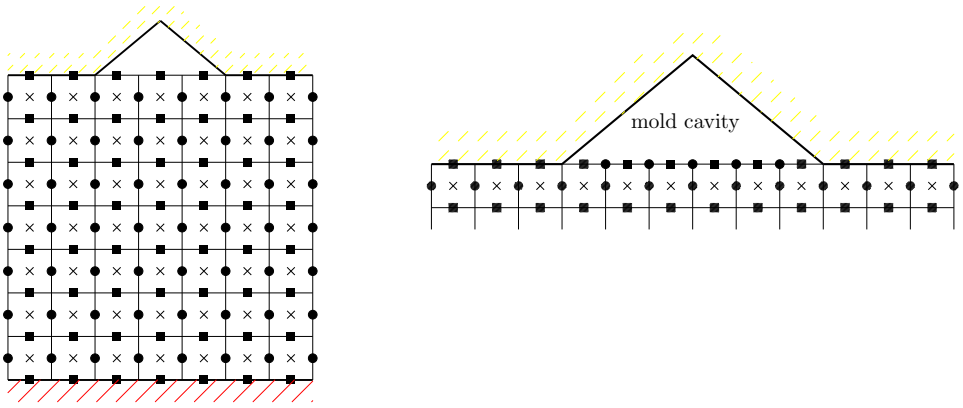

Figure 9 – Left: MAC mesh showing nodes for displacement in X direction (circles), Y direction (squares) and pressure (X marks). Right: free boundary nodes for displacement (solid) and their interaction with the rest of the nodes.

computation of the pressure around the endpoints where the free surface is defined as well as the interaction of the free surface with the mold, which forced us to seek a more sophisticated scheme to compute the pressure and displacements on these nodes (Fig. 9).

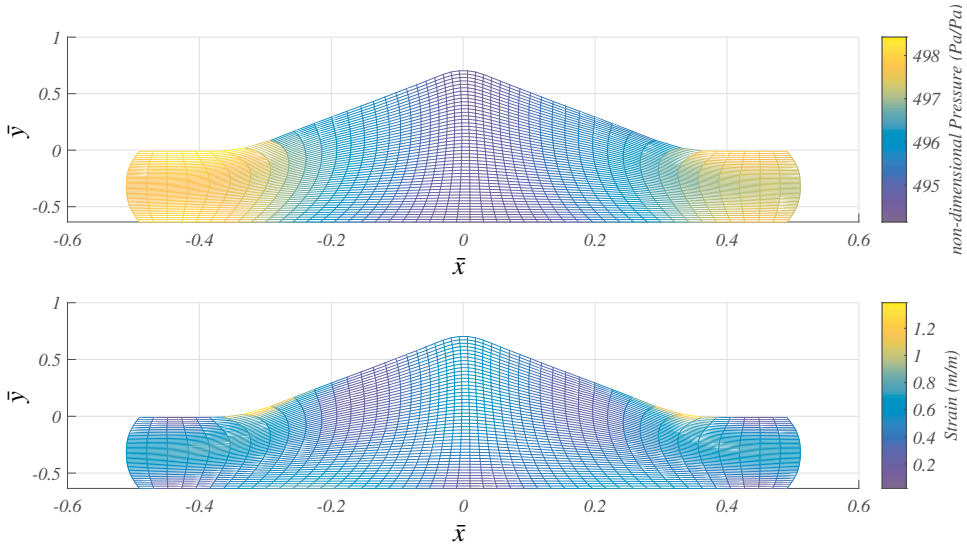

Figure 10 – Pressure and strain distributions at the end of the available time for filling $\bar{t} = 1$

The pressure and strain fields at time $t = T_1$ are shown in Fig. 10. Large strain zones are observed near the edges where the free surface begins, i.e., the inner zone around the mold feature, and two symmetrical zones attached on the substrate. Because the behavior is more elastic in these zones, the material is

most likely to snap back to its previous state, and could cause contractions and undesirable deformations during the phase change. Higher pressures are observed on the sides since the fluid is being pushed up in the center of the domain with very little variation across the thickness of the fluid film. The pressure field that is observed in the simulations is qualitatively consistent with the assumptions made in the existing models, with the crucial difference being that the pressure distributions observed in this paper are the result of numerical implementation of conservation laws and not as a consequence of a priori assumptions. In essence, the pressure difference at the end of mold filling could be one of the main sources of energy affecting the final geometry after the phase change occurs.

In the following, we discuss the numerical simulations and evolution of the mold filling process in terms of web speed, fluid film thickness, material properties. Although one would ideally describe this evolution in terms of the dimensionless numbers in the governing equations, for simplicity and as an initial step we have directly discussed the effects of web speed, film thickness, and material properties.

3.1 Effect of web speed

Figure 11 shows the evolution of the maximum and minimum strain magnitudes and corresponding vertical displacements for two different web speeds, 1 m/min and 90 m/min. The data are shown for points of maximum and minimum strain that typically occur on the edges where the free surface begins and at the midpoint of the domain, respectively, and points where the maximum and minimum displacement occur. Non-dimensional displacement variable is plotted so that both high and low web speeds can be placed on the same plot under the same (non-dimensional) time scale. At the higher speed of 90 m/min, the strain at the beginning clearly shows an almost linear elastic-like behavior which delays the displacement of the midpoint. At slow web speed the strain increase is almost linear up to the point where it fills the mold followed by a very smooth relaxation as opposed to the higher web speed case.

The displacement at the midpoint of the free surface inside the pattern is an indication of how well the mold is being filled; from numerical computations we observe that this occurs when the displacement ($u_s(t)$) is close to its steady-state value of $H-h$. Notice that the relative times $\bar{t}$ for both speeds at which their displacements become nearly constant determine the amount of fluid inside the mold. In addition, note that the pressure field increases at higher web speeds. This higher pressure field as well as "memory" at higher web speeds is what we conjecture as one of the main causes of unsatisfactory final geometry of the imprinted features.

3.2 Effect of fluid film thickness

The linearized model that we have employed imposes some restrictions in terms of the geometry of the mold that one can consider; the restrictions primarily are on the width to height ratio. Despite this restriction, we can observe some key qualitative behavior of the feature geometry within the mold. Since we assumed the fluid to be incompressible, the influence of changing the fluid film thickness ranges from unsatisfactory mold filling to bleeding of excess fluid to the sides (Fig. 12). This is an expected result given that we have explicitly stated the

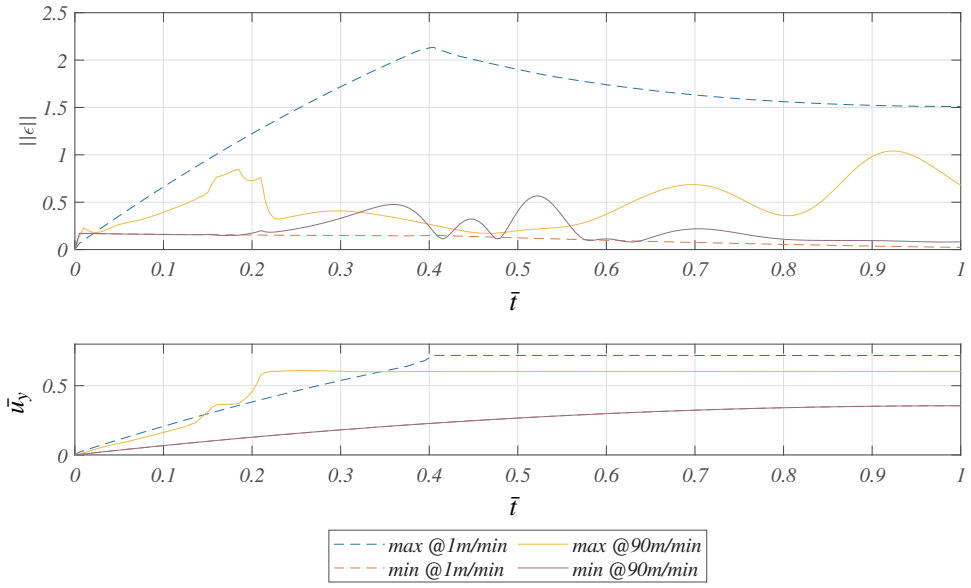

Figure 11 – Effects of high (solid) and low (dashed) web speeds on the linearized strain and the vertical displacement

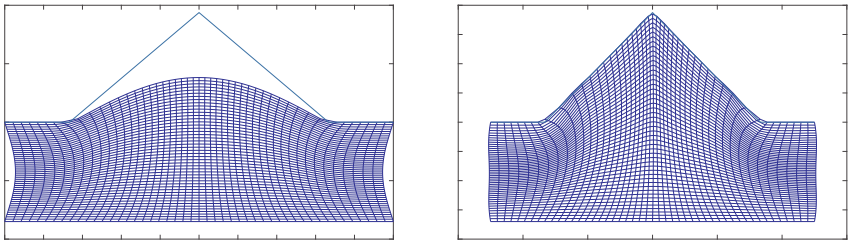

partially filled feature completely filled feature

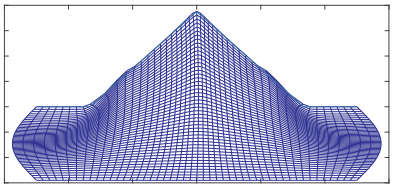

overfilled feature

Figure 12 – Effect of fluid film thickness

relationship between the geometry of the mold, the dimensions of the fluid film and the residual layer thickness (Eq. 6).

3.3 Effects of material properties

The fluid film properties of relevance are given by four parameters: density ρ, viscosity μ, stress-relaxation time λ and free surface energy γ. When the density increases, the fluid experiences almost no change since the Reynolds Number is very small compared to the other non-dimensional numbers. With increased viscosity, strain remains around the same values, but the pressure increases by around the same factor as that of the increase in viscosity, which may be consistent with the available experimental evidence. Results from numerical simulations suggest that the most important factor affecting mold filling may be the free-surface energy. When it increases, not only the fluid film is more susceptible to blockage into the mold pattern at higher web speeds, but it also increases the pressure field by several orders of magnitude; the scale-sensitivity of the model may be attributed to this aspect.

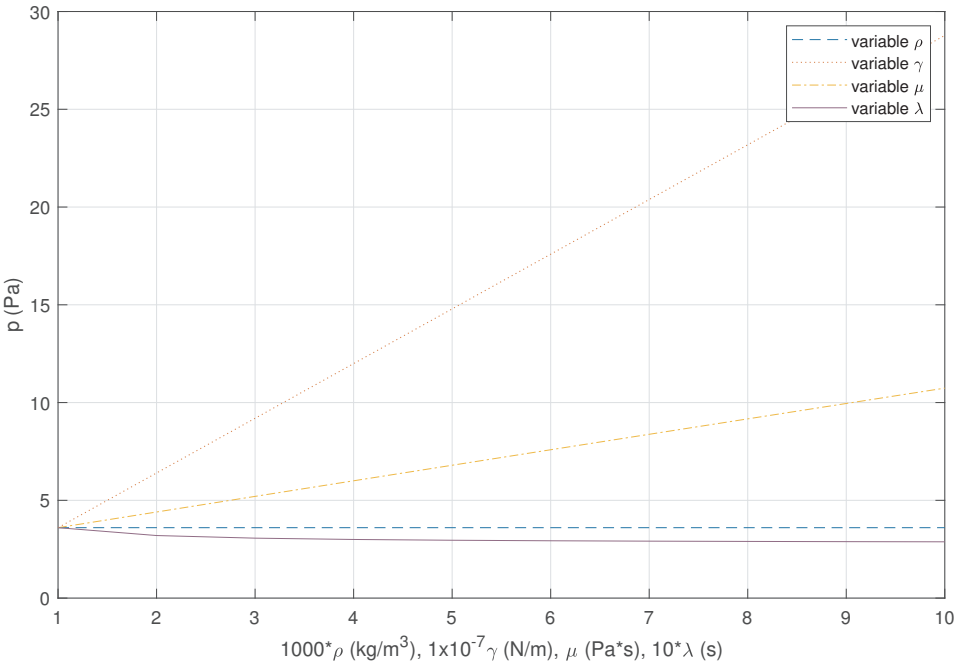

Figure 13 – Pressure variation in terms of the material properties

In summary, observations of the numerical simulations suggest that the most important factor related to the material properties when it comes to satisfactory mold filling is the interaction between the stress-relaxation time and the free surface energy. When both are increased, a surface tension force on the free surface is developed that prevents the fluid from filling the mold accompanied by a great increase in the pressure field by several orders of magnitude.

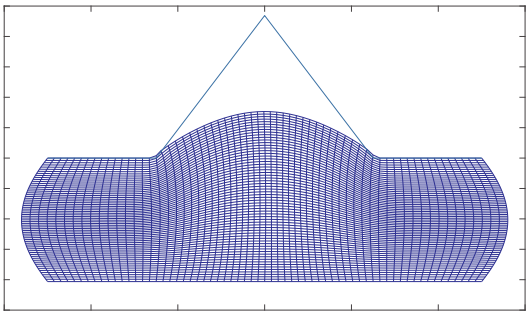

Figure 14 – Effect of the high stress-relaxation time and high free-surface energy on mold filling

4 CONCLUSIONS AND FUTURE WORK

During mold filling at higher speeds, we can observe elastic-like behavior for the fluid film followed by a slinky effect at higher speeds and ultimately presenting a clogging effect preventing the filling of the feature at very high speeds. The assumed linear viscoelastic behavior limits the range of mold geometries that can be considered, especially for features whose height is several times larger than the width. Despite this restriction, reasonable qualitative behavior of mold filling was observed.

Time-dependent pressure distribution was observed from numerical simulations of the governing equations. Since the observed pressure distributions are a result of application of conservation laws, the numerical results in this work are more realistic than the existing results where a priori assumptions are made on the pressure distributions.

Mold filling is highly dependent on the interactions between the material properties, especially the stress-relaxation time λ and free-surface energy γ. This provides opportunities for considering more suitable materials for nanoimprinting with lower free-surface energy and stress-relaxation time in order to improve the mold filling process; these materials could potentially replace expensive extra steps of using ferromagnetic particles and magnetic mold rollers to increase mold filling at higher speeds.

In this paper we assumed a simple constitutive material law that still captures the viscoelastic behavior. Depending on the complexity and the desired accuracy needed for a given application, one can consider more complex constitutive relations that could capture mold filling more accurately.

The results obtained using this model also provide insights and initial conditions for the subsequent phase change process of the mold pattern. The phase change must take into account the pressure distribution and the strain in the mold pattern at the end of the available time for filling (T_1). The main difference between the two sub-processes arises from the different boundary conditions, namely the tension on the substrate and several other additional

factors which will be considered as part of the future work.

ACKNOWLEDGEMENTS

This work was supported in part by the NSF grant number 1635636.

REFERENCES

1. Bird, R.B., Armstrong, R.C. and Hassager, O., "Dynamics of polymeric liquids. Vol. 1: Fluid mechanics" John Wiley and Sons Inc., Volume 1, 2nd edition, 1987.
2. Schift, H. and Heyderman, L.J., "Alternative Lithography: Unleashing the Potentials of Nanotechnology" C.M. Sotomayor Torres, Ed., Kluwer Academic/Plenum Publishers, pp 47-76, 2003.
3. Kim, N.W., Kim, K.W. and Sin, H.C., "A mathematical model for slip phenomenon in a cavity-filling process of nanoimprint lithography" Microelectronic Engineering, Volume 86, N 11 ,p 2324-2329, Elsevier, 2009.
4. Young, W.B., "Analysis of the nanoimprint lithography with a viscous model" Microelectronic Engineering, Volume 77, N 3-4, pp 405-411, Elsevier, 2005.
5. Ahn, S.H. and Guo, L.J., "Large-area roll-to-roll and roll-to-plate nanoimprint lithography: a step toward high-throughput application of continuous nanoimprinting" ACS nano, Volume 3, N 8, pp 2304-2310, ACS Publications, 2009.
6. Jain, A. and Bonnecaze, R.T., "Fluid management in roll-to-roll nanoimprint lithography" Journal of Applied Physics, Volume 113, N 23, p. 234511, AIP, 2013.
7. Jain, A., "Simulation of UV nanoimprint lithography on rigid and flexible substrates" PhD Thesis, The University of Texas at Austin, TX, pp 9, 2016.
8. Thesen M.W., Rumler, M., Schlachter, F., GrÃijtzner, S., Moormann, C., Rommel, M., Nees, D., Ruttloff, S., Pfirrmann, S., Vogler, M. and Schleunitz, A. , "Enabling large area and high throughput roll-to-roll NIL by novel inkjetable and photo-curable NIL resists." Alternative Lithographic Technologies VI, Volume 9049, p. 90490H, International Society for Optics and Photonics, 2014.
9. Thesen M.W., Nees, D., Ruttloff, S., Rumler, M., Rommel, M., Schlachter, F., Grützner, S., Vogler, M., Schleunitz, A., and Grützner, G., "Inkjetable and photo-curable resists for large-area and high-throughput roll-to-roll nanoimprint lithography." Journal of Micro/Nanolithography, N 4: p.043003, MEMS and MOEMS, 2014.
10. Wu, C.L., Sung, C.K„ Yao P.H., and Chen, C.H., "Sub-15 nm linewidth gratings using roll-to-roll nanoimprinting and plasma trimming to fabricate flexible wire-grid polarizers with low colour shift." Nanotechnology 24, N 26: p.265301, 2013.
11. Inanami, R. , Ojima, T., Matsuki, K., Kono, T. and Nakasugi, T., "Sub-100

nm pattern formation by roll-to-roll nanoimprint." Alternative Lithographic Technologies IV, Volume 8323, p. 832311, International Society for Optics and Photonics, 2012.

12. Ahn, S.H., Miller, M., Yang, S., Ganapathisubramanian, M., Menezes, M., Singh, V., Choi, J, Xu, F., LaBrake, D., Resnick, D.J. and Sreenivasan, S.V., "High volume nanoscale roll-based imprinting using jet and flash imprint lithography." Nanoengineering: Fabrication, Properties, Optics, and Devices X, Volume 8816, p. 881602, International Society for Optics and Photonics, 2013.

13. Ahn, S., Ganapathisubramanian, M., Miller, M., Yang, J., Choi, J., Xu, F., Resnick, D.J. and Sreenivasan, S.V., "Roll-to-roll nanopatterning using jet and flash imprint lithography." Alternative Lithographic Technologies IV, Volume 8323, p. 83231L, International Society for Optics and Photonics, 2012.

14. Mäkelä, T., Haatainen, T., and Ahopelto J., "Roll-to-roll printed gratings in cellulose acetate web using novel nanoimprinting device." Microelectronic Engineering, Volume 88, pp 2045-2047, 2011.

15. Sohn, K.J., Park J.H., Lee, D.E., Jang, H.I. and Lee, W.I., "Effects of the process temperature and rolling speed on the thermal roll-to-roll imprint lithography of flexible polycarbonate film." Journal of Micromechanics and Microengineering, Volume 23,(3),p. 035024, 2011.

16. Macosko, C.W. and Larson, R.G., "Rheology: principles, measurements, and applications." VCH New York, pp. 109, 1994.

17. Wineman, A.S. and Rajagopal, K.R., "Mechanical response of polymers: an introduction." Cambridge university press, pp. 148, 2000.

18. Poole, R.J., "The Deborah and Weissenberg numbers." Rheology Bulletin., pp. 32-39, The British Society of Rheology, 2012.

19. Harlow, F.H. and Welch, J.E., "Numerical calculation of time-dependent viscous incompressible flow of fluid with a free surface." Physics of Fluids., Vol 8, pp. 2182-2189, 1965.